Ionothermal carbonization in [Bmim][FeCl 4]: an opportunity for the valorization of raw lignocellulosic agrowastes into advanced porous carbons for CO 2 capture

Laure Cibien, Maxime Parot, Patrick Nkuigue Fotsing, Philippe Gaveau, Emmanuel Djoufac Woumfo, Julien Vieillard, Alfredo Napoli, Nicolas Brun

▶ **To cite this version:**

Laure Cibien, Maxime Parot, Patrick Nkuigue Fotsing, Philippe Gaveau, Emmanuel Djoufac Woumfo, et al.. Ionothermal carbonization in [Bmim][FeCl 4]: an opportunity for the valorization of raw lignocellulosic agrowastes into advanced porous carbons for CO 2 capture. Green Chemistry, 2020, 22 (16), pp.5423-5436. 10.1039/d0gc01510e . hal-02935089

HAL Id: hal-02935089

https://hal.umontpellier.fr/hal-02935089

Submitted on 8 Dec 2020

HAL is a multi-disciplinary open access archive for the deposit and dissemination of scientific research documents, whether they are published or not. The documents may come from teaching and research institutions in France or abroad, or from public or private research centers.

L'archive ouverte pluridisciplinaire **HAL**, est destinée au dépôt et à la diffusion de documents scientifiques de niveau recherche, publiés ou non, émanant des établissements d'enseignement et de recherche français ou étrangers, des laboratoires publics ou privés.

Ionothermal Carbonization in [Bmim][$FeCl_4$]: an Opportunity for the Valorization of Raw Lignocellulosic Agrowastes into Advanced Porous Carbons for CO_2 Capture†

Laure Cibien,[‡,1] Maxime Parot, [‡,1] Patrick Nkuigue Fotsing,[2] Philippe Gaveau,[1] Emmanuel Djoufac Woumfo,[2] Julien Vieillard,[3] Alfredo Napoli,[4] Nicolas Brun*[,1]

[1]ICGM, Univ Montpellier, CNRS, ENSCM, Montpellier (France)

[2]Laboratoire de Chimie Inorganique Appliquée, Département de Chimie Inorganique, Faculté des Sciences, Université de Yaoundé I, Yaoundé (Cameroun)

[3]Normandie Univ., UNIROUEN, INSA Rouen, CNRS, COBRA (UMR 6014), Rouen (France)

[4]CIRAD, UR BioWooeb, Montpellier (France)

*Email: nicolas.brun@enscm.fr

†Electronic Supplementary Information (ESI) available: [Additional analytical data]. See DOI: 10.1039/x0xx00000x

‡These authors contributed equally to this work

Abstract

In this study, we investigated the ionothermal carbonization (ITC) in 1-butyl-3-methylimidazolium tetrachloroferrate, [Bmim][$FeCl_4$], of cocoa bean shells, a raw lignocellulosic agrowaste. The beneficial inputs of this ITC approach towards mass yield, carbon yield and specific surface area of the solid chars (namely, ionochars) were clearly evidenced. The coordination of $[FeCl_4]^-$ anions to the oxygen atoms of lignocellulosic materials and ionochars seems to stabilize carbon oxygenated groups – accounting for enhanced mass and carbon yields – and to favor the generation of micropores. We showed that the use of wet starting agrowastes in the ITC process might be advantageous for the production of highly porous ionochars. Importantly, the contributions of lignin and cellulose were highlighted and the recyclability of [Bmim][$FeCl_4$] was clearly evidenced, proving the sustainability of ITC and making this process easily applicable to other raw lignocellulosic agrowastes. The subsequent activation of the as-obtained ionochars under CO_2-rich atmosphere allowed producing activated carbons with specific surface area superior to 2000 $m^2.g^{-1}$ and remarkable CO_2 uptake as high as 4.4 $mmol.g^{-1}$ at 25°C and 1 bar. This value is the highest post-combustion CO_2 uptake reported to date in literature for CO_2 activated biomass-derived carbons.

Graphical Abstract

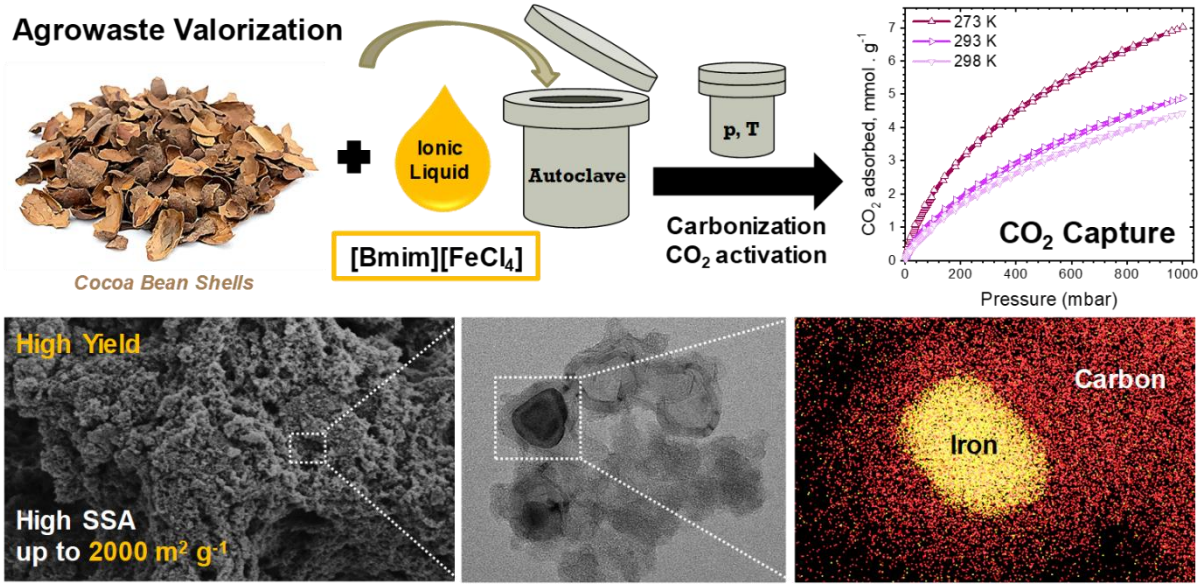

1. Introduction

With the concept of biorefinery, the conversion of renewable feedstocks into energy and marketable products, *e.g.* platform chemicals and advanced materials, has constituted a major field of research.[1, 2] This assessment is particularly true for the agro-industry sector, which generates a large amount of organic residues, namely agrowastes. These agrowastes are cheap, renewable and abundant, making them attractive raw materials for sustainable industrial processes. Amongst biorefinery's end products, porous carbonaceous materials[3, 4] have attracted much interest as they offer a wide range of potential applications in energy storage,[5, 6] catalysis[7] and environmental remediation[8-10]. Until relatively recently, the thermochemical conversion of renewable feedstocks into porous carbons was limited to dry pyrolysis and/or activation processes. In the past years, wet pyrolysis in water, also called hydrothermal carbonization (HTC), has been seen as a promising alternative to design porous carbonaceous materials on demand from renewable feedstocks.[11-16] Those carbonaceous materials, also called hydrochars, can be obtained from a large range of natural precursors, including untapped byproducts generated during degradation of lignocellulose in paper mills[17] and biorefineries[6]. The hydrothermal approach is based on the degradation/dehydration of (poly)saccharides into furan-based intermediates at relatively mild conditions; typically at a temperature between 130 and 250°C and at a pressure below 10 bars. HTC usually yields microscopic nonporous spheres with limited control over morphology and texture. When applied to soluble carbohydrates, *e.g.* monosacharides, HTC has been frequently combined with sacrificial templates[18-23], catalysts and/or structuring agents[24-27] to yield porous hydrochars. Conversely, the hydrothermal carbonization of insoluble feedstocks, *e.g.* cellulose and raw lignocellulosic materials, remains limited in terms of textural and morphological control.[13]

Since 2002 and the first article demonstrating their ability to dissolve cellulose,[28] ionic liquids (ILs) have been widely employed in biorefinery, both as derivatizing[29-31] and nonderivatizing[28, 32] solvents. Particularly, short-chain imidazolium-based room temperature ILs with strong hydrogen bond acceptors as anions, such as 1-butyl-3-methylimidazolium chloride (*i.e.* [Bmim]Cl), appeared to be very efficient in solubilizing cellulose. R.D. Rogers *et al.* demonstrated that such solvation involves stoichiometric hydrogen-bonding between the hydroxyl protons of the polysaccharide and the anions of the IL.[28, 33] From that moment on, few other hydrophilic ILs, with various anions (*e.g.* chloride, phosphate, phosphonate and acetate) and cations (*e.g.* imidazolium, ammonium and phosphonium), demonstrated similar

abilities.[34] While the role of the anion seems to be clear (*i.e.* related to hydrogen bonding basicity), the way cationic structure affects the dissolution of cellulose is still open to discussion.[35] Besides, functional ILs with acidic properties have been employed both as solvent and catalyst for the hydrolysis and conversion of lignocellulosic biomass to platform chemicals.[36-38]

Beyond dissolution and selective deconstruction, ILs were also employed for the thermochemical conversion of carbohydrates into porous carbonaceous materials. Usually, ionic liquid is involved either as a soft-template in water[39, 40] or as a functional solvent playing the role of catalyst and/or porogenic agent [41-44]. While the first approach falls in the category of HTC, the second one can be regarded as ionothermal carbonization (ITC; by analogy with hydrothermal carbonization) yielding ionochars (by analogy with hydrochars). While full of promise, the ITC process is still a young topic with reaction mechanisms yet to elucidate and a limitless variety of carbon precursor/IL systems to investigate. Thus far, such ionothermal treatment has not been fully exploited and was mainly restricted to monosaccharides,[42-44] except for rare examples dealing with raw lignocellulosic agrowastes[45, 46]. Using Bmim-type ILs with different anions (*i.e.* Cl^-, BF_4^- and Tf_2N^-), Wang *et al.*[45] applied the ITC process to cellulose and sugar cane bagasse. The authors showed a correlation between the size of the anion and the textural properties of the ionochar – *i.e.* larger anions yield higher pore volume – revealing a bit more the versatility of the ITC process. More recently, Xie *et al.*[46] applied the ITC approach to Jujun grass. After treatment at 180°C in a Lewis acid ionic liquid (*i.e.* 1-butyl-3-methylimidazolium tetrachloroferrate, [Bmim][$FeCl_4$]) and subsequent chemical activation with KOH, the authors obtained hierarchical porous carbons with high surface area and significant mesoporous contribution. The beneficial input of the ITC pre-treatment in terms of porosity and capacitive performance was clearly evidenced, making this two-step approach really promising. However, in this last study, the authors considered ionochars as synthetic intermediates and mainly focused on the final activated carbons and their electrochemical properties. More recently, X. Li *et al.*[47, 48] demonstrated synergistic effects that make [Bmim][$FeCl_4$] an efficient catalyst for the depolymerization of lignin through γ-O ester bond cleavage. Even though the authors focused on the production of methyl p-hydroxycinnamate, a platform molecule for a variety of fine chemicals, rather than on the production of ionochars, this study further supported the relevance of using [Bmim][$FeCl_4$] for the conversion of lignocellulosic materials.

In this study, we propose to provide further insights into the ITC process applied to lignocellulosic biomass *via* thorough textural and structural characterizations and comparison with hydrochars analogous. With this aim, we applied the ITC approach to a raw lignocellulosic agrowaste model, *i.e.* cocoa bean shells (CS) from Cameroon. The cocoa industry is a pertinent model as it generates a large amount of agrowastes. Through on-farm processing, *ca.* 80 wt.% of the cocoa fruit is discarded as residues, including cocoa pod husk, cocoa pulp and CS.[49] Herein, both [Bmim]Cl, a well-known commercial ionic liquid, and [Bmim][$FeCl_4$], a Lewis acid ionic liquid analogous, were employed as reaction media for the treatment of CS. The beneficial inputs of the ITC approach towards mass yield, carbon yield and specific surface area were clearly evidenced. Importantly, the contributions of lignin and cellulose were highlighted and the recyclability of [Bmim][$FeCl_4$] was clearly evidenced, proving the sustainability of the ITC approach and making this process easily applicable to other raw agrowastes. The subsequent activation of the as-obtained ionochars with carbon dioxide allowed producing activated carbons with specific surface area superior to 2000 $m^2.g^{-1}$ and remarkable CO_2 uptake as high as 4.4 $mmol.g^{-1}$ at 25°C and 1 bar. This value is amongst the highest values reported to date in literature for nitrogen-free biomass-derived carbons. In this contribution, we wish to provide useful insight and understanding of the transformation mechanism involved in the ITC of lignocellulosic biomass in [Bmim][$FeCl_4$]. Besides, we believe that this study further contributes to demonstrate that ITC can be a promising approach into the circular economy for the valorization of raw agrowastes into advanced carbonaceous materials.

2. Experimental section

2.1. Materials

Iron (III) chloride hexahydrate was purchased from Acros Organics. 1-Butyl-3-methylimidazolium chloride (99 %) was purchased from Iolitec (Germany) and kept under vacuum to avoid hydration. Sigmacell cellulose (type 50, 50 µm) and kraft lignin were purchased from Sigma Aldrich. All reagents were used without further purification.

2.2. Preparation of the cocoa bean shells (CS)

The cocoa bean shells (CS) were collected from a local farm managed by the IRAD (Institute of Agricultural Research for Development) at Yaoundé, Cameroon. The shells were cut, washed with acidic water (1M HCl) to remove organic matter, sun-dried for 5 days, and heated at 70°C overnight to remove moisture. Finally, CS were ground and sifted at 160 µm.

2.3. Extraction of lignin by the Klason method

Lignin was extracted from CS and quantified using the Klason method as described in literature.[50] In brief, 3 g of CS were treated in 30 mL of concentrated sulfuric acid (72 wt.% H_2SO_4) at 25 °C for 1 hour under vigorous stirring. The slurry was diluted with deionized water to decrease the H_2SO_4 concentration to 4 wt.%, autoclaved at 121 °C for 60 min and filtrated through a 0.22 µm PVDF membrane. The insoluble lignin fraction, namely Klason lignin (KL), was dried at 100°C overnight in a vacuum oven and weighed. The ash content was determined by thermogravimetric analysis under a dry air atmosphere. The soluble lignin fraction was quantified by UV–vis spectroscopy.

2.4. Hydrothermal carbonization (HTC)

Typically, CS powder (1 g) was dispersed in deionized water (10 mL), sealed in a Teflon lined autoclave (37 mL) and heated at 240 °C for 20 h. After cooling down to room temperature (through quenching in cold water), samples were filtered, successively washed two times with deionized water (50 mL) and two times with ethanol (50 mL), then dried at 80 °C overnight. The as-obtained samples were named **HC-240**. Similar experiments were carried out in the presence of $FeCl_3$. $FeCl_3.6H_2O$ (10.86 g, corresponding to 40.2 mmol of $FeCl_3$) was mixed with deionized water (c.a. 4 mL) until the gauge of a 10 mL volumetric flask was reached. The 10 mL solution was mixed with CS powder (1 g) and sealed in a Teflon lined autoclave (37 mL) and heated at 240 °C for 20 h. After filtration, washing and drying, the as-obtained samples were named **HC-Fe-240**.

2.5. Ionothermal carbonization (ITC)

2.5.1. ITC in [Bmim]Cl

Typically, CS powder (1 g) was mixed with [Bmim]Cl (10.8 g), sealed in a Teflon lined autoclave (37 mL) and heated at 240 °C for 20 h. After cooling down to room temperature (through quenching in cold water), samples were filtered, successively washed two times with deionized water (50 mL) and two times with ethanol (50 mL), then dried at 80 °C overnight. The as-obtained samples were named **IC-240**.

2.5.2. Preparation of [Bmim][$FeCl_4$]

[Bmim][$FeCl_4$] was prepared using the well-established procedure reported in literature.[42, 51] Typically, equimolar amounts of $FeCl_3.6H_2O$ (64.86 g, 0.24 mol) and [Bmim]Cl (41.92 g,

0.24 mol) were mixed in a round-bottom flask for 30 min at room temperature under vigorous stirring. [Bmim][$FeCl_4$] was then dried under vacuum at 100 °C overnight.

2.5.3. ITC in [Bmim][$FeCl_4$]

Typically, CS (1 g) was dispersed in [Bmim][$FeCl_4$] (13.56 g, c.a. 10 mL and 40.2 mmol), sealed in a Teflon lined autoclave (37 mL) and heated at 240 °C for 20 h. After cooling down to room temperature (through quenching in cold water), samples were filtered, successively washed two times with deionized water (50 mL) and two times with ethanol (50 mL), then dried at 80 °C overnight. The as-obtained samples were named **IC-Fe-240**. Some experiments were conducted in 10 mL of [Bmim][$FeCl_4$]/water mixtures. The as-obtained samples were named **IC-Fe-240-*y*w**, where *y* is the water content in wt.%.

All experiments were performed at least in triplicate. All the data reported in this study correspond to average values. Standard deviation was used to measure the statistical dispersion and error bars were included on all graphs accordingly.

2.6. High temperature post-treatment

2.6.1. Pyrolysis

Pyrolysis was carried out in a horizontal tube furnace at 900 °C for 2 h with a heating rate of 5 °C min^{-1} under argon flow (50 mL min^{-1}). Samples were then allowed to cool down to room temperature through a natural convection step. The as-obtained samples were named with the suffix **P9**.

2.6.2. CO_2 activation

CO_2 activation was carried out in a vertical tube furnace following two different procedures.

In a first procedure, the samples were pretreated at 950 °C for 10 min under nitrogen flow (100 mL min^{-1}) with a heating rate of 10 °C min^{-1} and an intermediate drying plateau at 110°C for 60 min, and subsequently treated at 950°C for 120 min under a CO_2 enriched nitrogen flow (10 mL min^{-1} CO_2, 90 mL min^{-1} N_2). The as-obtained samples were named with the suffix **A1**.

In a second procedure, the samples were treated at 950 °C for 130 min under a CO_2 enriched nitrogen flow (10 mL min^{-1} CO_2, 90 mL min^{-1} N_2) with a heating rate of 10 °C min^{-1} and an

intermediate drying plateau at 110°C for 60 min. The as-obtained samples were named with the suffix **A2**.

In all cases, samples were allowed to cool down to room temperature through a natural convection step.

2.7. Mass and carbon yields

The mass yield and the corrected mass yield were calculated as follows:

$$\textbf{\textit{Mass yield}}\ (\%) = \frac{\textbf{\textit{Mass of dried char}}\ (\textbf{\textit{g}})}{\textbf{\textit{Mass of dried initial biomass}}\ (\textbf{\textit{g}})} \times \mathbf{100}$$

$$\textbf{\textit{Corrected Mass yield}}\ (\%) = \frac{\textbf{\textit{Mass of dried char}}\ (\textbf{\textit{g}}) - \textbf{\textit{Mass of residual atoms}}\ (\textbf{\textit{g}})}{\textbf{\textit{Mass of dried initial biomass}}\ (\textbf{\textit{g}})} \times \mathbf{100}$$

Residual atoms correspond to any atom present in the dried char and coming from the salt ($FeCl_3$) or the ionic liquid ([Bmim]Cl or [Bmim][$FeCl_4$]), *i.e.*, iron, chloride and nitrogen excess. Iron and chloride contents were determined by SEM-EDX (**section 2.7**). Nitrogen content was determined by elemental analysis. The nitrogen excess coming from the ionic liquid was determined by subtracting the nitrogen coming form the initial biomass. **HC-240** and **HC-180** were used as references.

The carbon yield was calculated as follows:

$$\textbf{\textit{Carbon yield}}\ (\%) = \textbf{\textit{Mass yield}}\ (\%) \times \frac{\textbf{\textit{C content in dried char}}\ (\textbf{\textit{wt.}}\%)}{\textbf{\textit{C content in dried initial biomass}}\ (\textbf{\textit{wt.}}\%)} \times \mathbf{100}$$

2.8. Characterization

Scanning electron microscopy (SEM) analyses were performed on a Hitachi S-4800 electron microscope. SEM-EDX (Energy Dispersive X-ray spectroscopy) analyses were performed on a Zeiss EVO HD15 electron microscope. Transmission electron microscopy (TEM) analyses were performed on a JEOL 1200 microscope. High resolution TEM analysis was performed on a JEOL 2200FS microscope operated at 200 kV, from the MEA platform (Université de Montpellier). This microscope is equipped with a field emission gun (FEG) and an in-column Omega-type energy filter. STEM-EDX (Scanning Transmission Electron Microscopy) mapping were performed using a probe size of 1.5 nm and X-rays measured with a silicon drift detector (30 mm^2, JEOL) with a collection solid angle of 0.13sr. N_2 (at 77 K) and CO_2 (at 273, 293 and 298 K) physisorption experiments were carried out on a Micromeritics 3Flex

apparatus. Ionochars and hydrochars were degassed at 150 °C and carbons (*i.e.*, materials post-treated at high temperature) were degassed at 250 °C for 6 h under high vacuum (*ca.* 0.1 Pa) before physisorption measurements. ^{13}C solid-state NMR was carried out on a VARIAN VNMRS 300 MHz spectrometer at 75.44 MHz. A VARIAN T3 MAS probe was used with 3.2 mm ZrO_2 rotors. Experiments were performed using Cross Polarization Magic Angle Spinning (CP-MAS) with a contact time of 1 ms and a recycle delay of 5 s. Rotors were spun at 15 kHz. Plastic inserts were removed from the rotor and short caps were used to minimize the ^{13}C background signal. Spectra were normalized and the background signal was removed by subtracting the spectrum obtained with the empty rotor. FTIR spectroscopy was performed in attenuated total reflectance (ATR) mode on a PerkinElmer Spectrum Two spectrometer. XRD patterns were recorded on a Bruker D8 Advance diffractometer with a Bragg-Brentano geometry and equipped with a Bruker Lynx Eye detector, with the Kα radiation of Cu (λ = 1.5418 Å) and an angular step size of 0.02° into the 10°-80° interval. X-ray photoelectron spectroscopy (XPS) analyses were performed on a ESCALAB 250 ThermoElectron spectrometer using a monochromatized Al Kα source ($h\nu$ = 1486.6 eV) and a 500 µm spot size. GC-MS was performed on a Shimadzu QP2010SE gas chromatograph-mass spectrometer with a Phenomenex Zebron ZB-5ms column (30m x 0.18mm x 0.18µm). Injection: Split 1:30 @ 250 °C. Oven program: 50 °C (hold 2 min) 50-280 °C @ 22 °C/min (Hold 2 min). Thermogravimetric analyses (TGA) were carried out using a Netzsch Simultaneous Thermal Analyzer STA 409 PC Luxx, with a heating rate of 10 °C min^{-1} in the 20-1000 °C range, under a dry air atmosphere (50 mL min^{-1}).

3. Results and discussion

3.1. Ionothermal (ITC) *versus* hydrothermal (HTC) carbonization

In the manner of hydrothermal carbonization (HTC), ionothermal carbonization (ITC) is a thermochemical process which allows carbonization of carbohydrates and raw lignocellulosic materials under mild conditions (*i.e.* < 10 bars and < 240 °C).[12, 13] ITC of carbohydrates in [Bmim][$FeCl_4$] (**BFe**) was previously described by Xie *et al.*, and the multiple role played by this iron-containing IL was clearly evidenced.[42] $FeCl_3$ acts as a Lewis acid catalyst involved in the different stages of the carbonization process. Its combination with [Bmim]Cl yields a room-temperature IL which acts as a porogen and as a solvent with good moisture-stability and superior solvation properties compared to water. Thus, ITC of carbohydrates in **BFe** generated porous ionochars with a higher carbonization yield compared with analogous

hydrochars obtained by the HTC process. These features were confirmed in our study with raw biomass, *i.e.*, cocoa bean shell (CS). CS is an abundant and often underexploited lignocellulosic agrowaste from the cocoa industry that is mainly used as fuel for boilers or as fertilizer for cocoa trees.[49] The valorization of CS into valuable and marketable products will help improving waste disposal and developing local circular bioeconomy.[49, 52, 53] The cocoa shells employed in this study are constituted of ca. 25-30 wt.% lignin, ca. 55-60 wt.% holocellulose and ca. 6 wt.% ash (**Figure S1**, **Tables S1** and **S2**). **Figure 1a** represents the mass yield and the carbon yield for CS treated at 240°C for 20 hours in water (**HC-240**), in water with $FeCl_3$ (**HC-Fe-240**), in [Bmim]Cl (**IC-240**) and in **BFe** (**IC-Fe-240**). Both mass yield (43.4 wt.%) and carbon yield (73 wt.%) were significantly improved for **IC-Fe-240** as compared with its analogous obtained in water or in [Bmim]Cl (**Table S3**). Similarly, the textural properties of **IC-Fe-240** were significantly improved. The nitrogen sorption isotherms obtained at 77 K are shown in **Figure 2b**. **IC-Fe-240** displays a type I/II isotherm with a H3 hysteresis loop, related to micro-macroporous materials. This ionochar is mainly microporous with a BET equivalent specific surface area (SSA_{BET}) of 550 $m^2.g^{-1}$ (**Figure 1c** and **Table S4**). A similar shape was obtained for **HC-Fe-240**. This hydrochar presents a high SSA_{BET} of 284 $m^2.g^{-1}$ with equal SSA contributions from micropores and macropores (**Figure 1c** and **Table S4**). On the contrary, **HC-240** depicts a type II isotherm, typical of macroporous materials, with a low SSA_{BET} of 20 $m^2.g^{-1}$, while **IC-240** is non-porous. These observations were confirmed by scanning (SEM, **Figure S2**) and transmission electron microscopy (TEM, **Figure 2**). As shown by TEM (**Figure 2a**), **HC-240** is made of aggregated nanoparticles with a diameter of ca. 50-100 nm. These particles are mainly not dispersible and supported on the preserved natural macrostructure of the native CS (**Figure S2**). As for **IC-240**, SEM observations confirm the absence of porosity even at the macroscopic scale (**Figure S2**). As shown by SEM and TEM, the presence of iron chloride either in water or in **BFe**, significantly affects the nanoparticle size. **HC-Fe-240** (**Figure 2b**) and **IC-Fe-240** (**Figure 2c**) are made of aggregated nanoparticles with smaller diameters of ca. 10-40 nm, in good agreement with the higher external SSA obtained by nitrogen sorption analyses (**Figure 1**). These results suggest that iron not only has a role of Lewis acid catalyst in the carbonization process, it is also involved in the generation of porosity. Importantly, a synergistic effect was clearly evidenced when processing ITC in **BFe**. **IC-Fe-240** shows improved mass yield, carbon yield and textural properties as compared with its two analogous obtained in the sole presence of [Bmim]Cl or $FeCl_3$ in water, *i.e.* **IC-240** and **HC-Fe-240** respectively. As suggested by Xie *et al.* for the ITC of carbohydrates,[42] **BFe** might closely interact with the biopolymers and the

carbonaceous particles through hydrogen bonds, but also *via* the π-system of the imidazolium ring. As imidazolium is amphiphilic, complex liquid structures might form[54] and favor the nucleation of small particles and the generation of meso- and macropores.

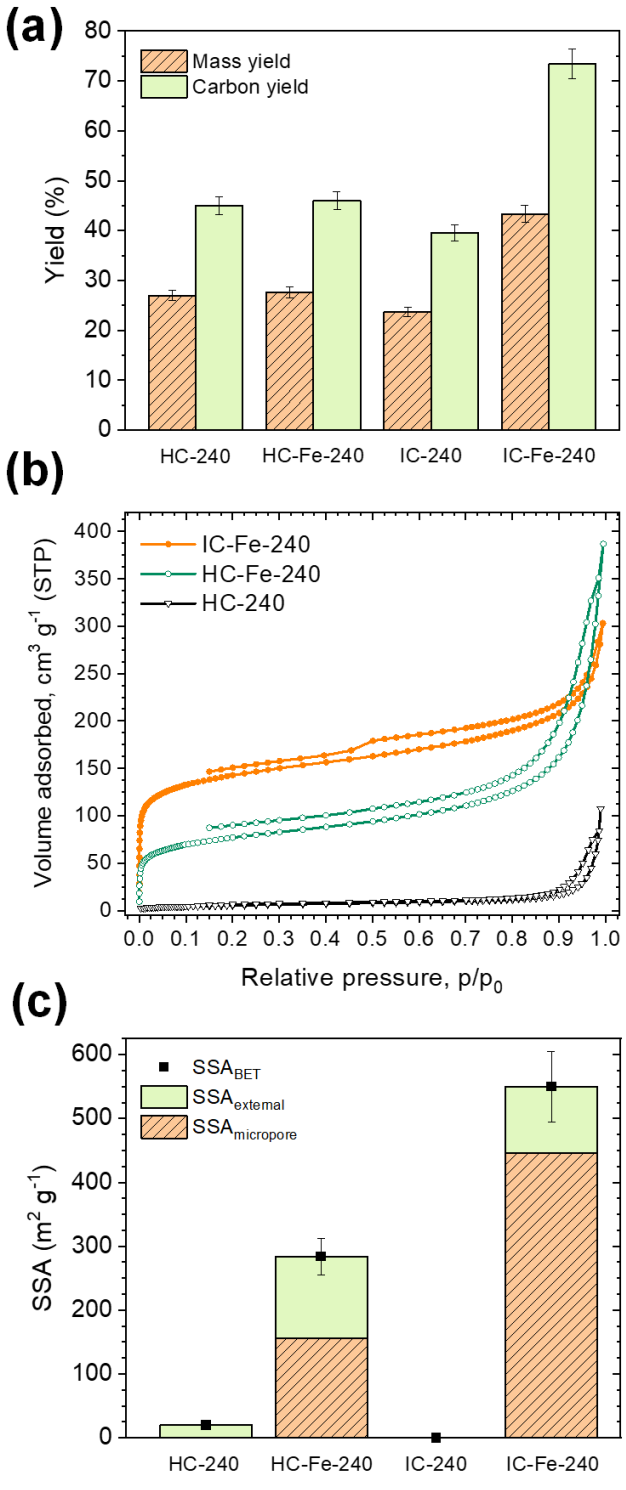

Figure 1. (a) Mass and carbon yields, (b) Nitrogen sorption isotherms at 77 K and (c) specific surface areas of **HC-240**, **HC-Fe-240**, **IC-240** and **IC-Fe-240**.

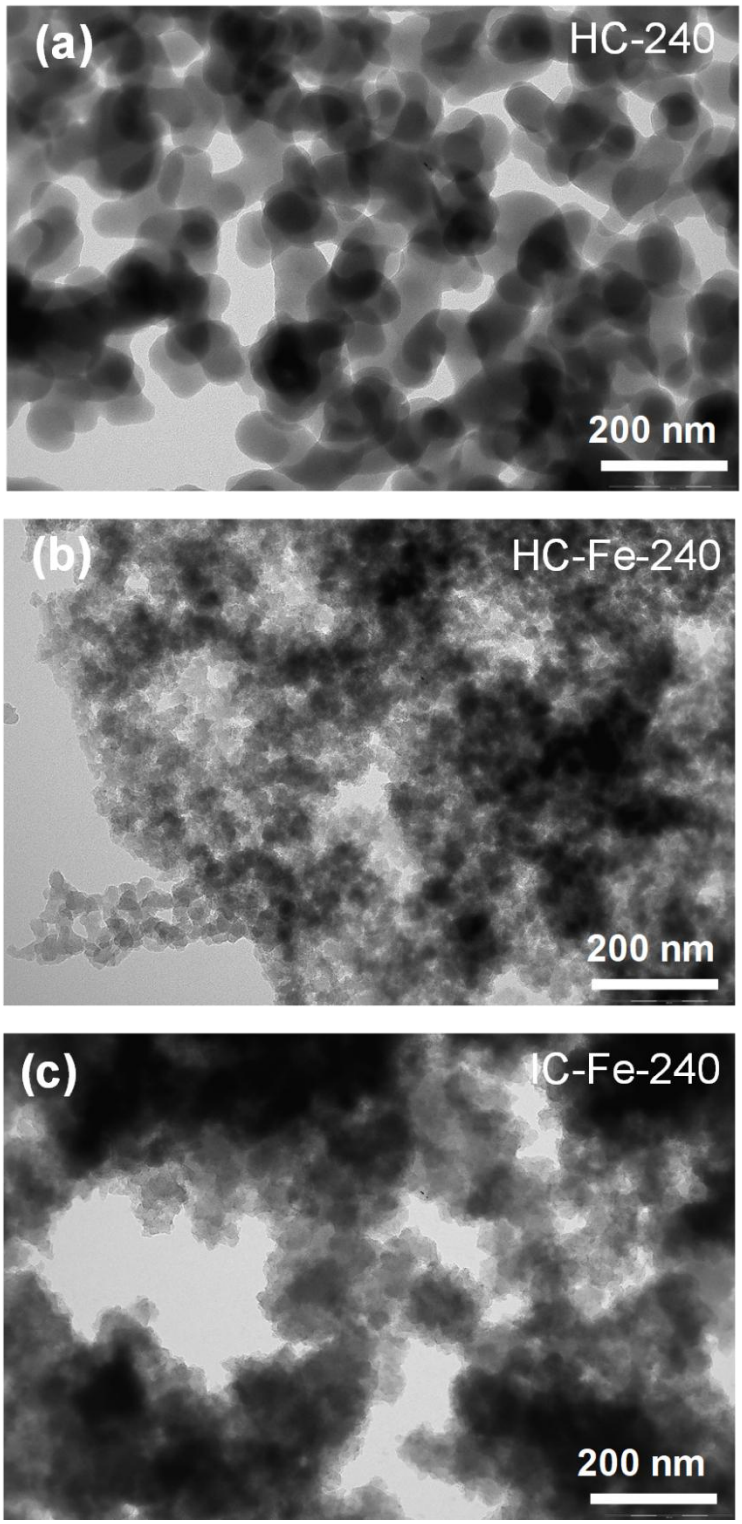

Figure 2. TEM micrographs of (a) **HC-240**, (b) **HC-Fe-240** and (c) **IC-Fe-240**.

The chemical structure of the four samples was investigated by FTIR (**Figure 3a**) and solid-state ^{13}C CP NMR spectroscopy (**Figure 3b**). **HC-Fe-240** and **IC-Fe-240** present similar FTIR spectra (**Figure 3a**) with two intense broad bands centered at 1600 (aromatic $\upsilon_{C=C}$ stretching vibrations) and 1220-1280 cm^{-1} (υ_{C-O} stretching vibrations in aromatic ethers and esters) and four shoulders centered at 1700 ($\upsilon_{C=O}$ stretching vibrations of aromatic carbonyl groups), 1440 (aromatic $\upsilon_{C=C}$ stretching vibrations), 1374 (δ_{CH3} bending vibrations of aromatic methyl groups) and 1074 cm^{-1}. These bands are mainly related to vibration modes in aromatic networks except for the one at 1074 cm^{-1}, which might correspond to alkoxy stretching vibrations (υ_{C-O}) of residual ester linkages between lignin and carbohydrates. **HC-240** and **IC-240** present similar FTIR spectra with three extra shoulders centered at 1040 (aromatic δ_{CH} in plane deformations), 1270 (υ_{C-O} stretching vibrations in lignin) and 1504 cm^{-1} (aromatic $\upsilon_{C=C}$ stretching vibrations in lignin). Moreover, the band centered at 1445 cm^{-1} is more intense. These bands can be attributed to the native ligneous components of CS. The band centered at 1040 cm^{-1} can be also attributed to υ_{C-O} stretching vibrations in holocellulose. These features suggest that lignin, and to a lesser extent holocellulose, are less affected in the absence of iron. The chemical structure of these four samples was also investigated by ^{13}C solid-state NMR spectroscopy (**Figure 3b**). Two major domains can be clearly identified: the aliphatic region between 0 and 50 ppm and the aromatic region centered at 120-125 ppm. At first glance, the two samples treated in the absence of iron, *i.e.* **HC-240** and **IC-240**, present more aliphatic carbons than **HC-Fe-240** and **IC-Fe-240**. This observation is particularly pronounced for **IC-240** with two narrow and intense peaks at 13 and 30 ppm and a shoulder at 19 ppm. This feature can be attributed to the partial degradation of [Bmim]Cl during the thermochemical treatment, as confirmed by GC-MS (**Figure S3**) and FTIR (**Figure S4**) of the recycled IL and by the presence of 6.7 wt.% of nitrogen in **IC-240** (**Table S3**). This will be further discussed in **section 3.4**. In the aromatic region, while **IC-240** displays a relatively narrow and intense peak centered at 122 ppm, **HC-240** and, to a lesser extent, **IC-Fe-240** and **HC-Fe-240,** present a shoulder centered at 145-150 ppm. This peak can be attributed to aromatic carbons bounded to lignin methoxy groups and suggests that lignin was mildly affected in these conditions. As for **HC-240**, this observation is in good agreement with FTIR spectroscopy. As for **HC-Fe-240** and **IC-Fe-240**, however, this feature is contradictory with the conclusions drawn from FTIR. As reported by Baccile *et al.*[12], the peak at 145-150 ppm can be also attributed to a nonsubstituted, protonated, α-carbon of the furan ring of furanic resins. At that stage, it is important to get back to basics of the HTC process applied to carbohydrates and lignocellulosic materials. The conversion of carbohydrates into hydrochars

is assumed to proceed in three main steps: (i) hydrolysis into monosaccharide units if starting from oligo- or polysaccharides, (ii) dehydration of monosaccharides into furan derivatives, and (iii) polycondensation of furan derivatives into polyfuranic species.[3, 12, 13, 15] At high temperature, typically at 240 °C, the carbonization process continues *via* intramolecular reactions (*i.e.*, condensation, dehydration and decarbonylation reactions) which lead to the production of condensed polyaromatic domains. As for insoluble feedstocks, e.g. cellulose and raw lignocellulosic materials, fundamental differences in the HTC mechanism were observed. As reported by Baccile et *al.*,[12, 13] the polyfuranic structures usually reported from simple carbohydrates cannot be observed in cellulose and lignocellulosic-derived hydrochars, which yield higher amounts of arene groups coming either from condensed furanic units or from polyaromatic hydrocarbon clusters. In this article, the authors concluded that the hydrolysis of cellulose to glucose and subsequent dehydration and polycondensation into polyfuranic species is limited to the cellulose-water interface and accounts for a minor part of cellulose conversion. Meanwhile, the HTC of bulky cellulose follows chemical reaction pathways comparable to the classical dry pyrolysis process. The results obtained herein with **HC-240** are in good agreement with the mechanism proposed by Baccile *et al.* based on hydrochars derived from cellulose and rye straw.

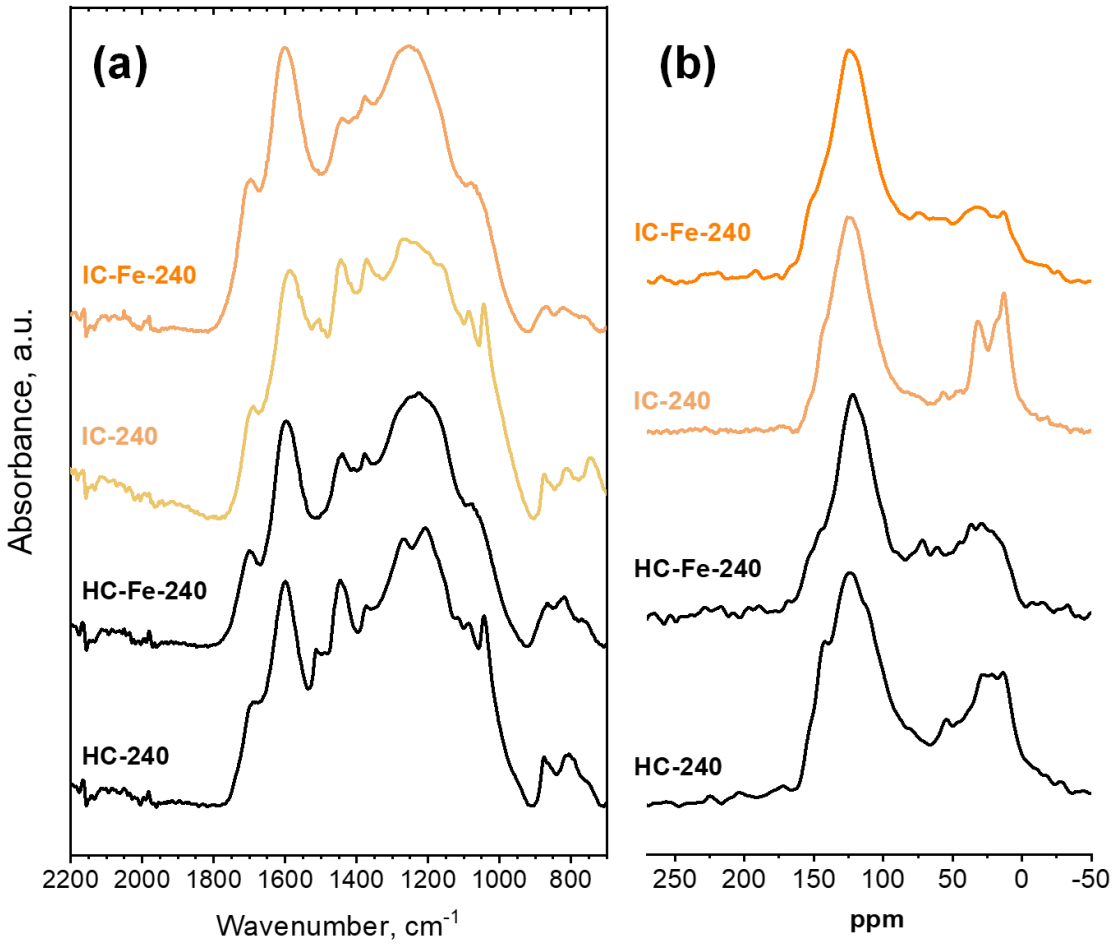

Figure 3. (a) FTIR and (b) ^{13}C CP-MAS NMR spectra of **HC-240**, **HC-Fe-240**, **IC-240** and **IC-Fe-240**.

Besides residual lignin, the presence of a shoulder at 145-150 ppm for **IC-Fe-240** can suggest a higher furan-to-arene ratio in the carbonaceous structure. This feature could be explained by a better solubility of the cellulosic component in IL that would increase the cellulose-solvent interface. One may expect a similar behavior in [Bmim]Cl. However, no clear shoulder was observed at 145-150 ppm for **IC-240**. Even though the presence of this peak is still a matter of discussion, the presence of oxygenated functional groups in the carbonaceous framework of **IC-Fe-240** was confirmed by elemental analyses (**Table S3**) and X-ray photoelectron spectroscopy (XPS, **Figures 4** and **S5**, **Tables S5** and **S6**). According to the simulated C1s XPS spectra, **IC-Fe-240** depicts less sp^2 carbons and more oxygenated functional groups than **HC-Fe-240** and **HC-240** (**Figure 4a**, **Table S5**). This behavior might be explained by the coordination of $[FeCl_4]^-$ to the oxygen atoms of carbohydrates and lignin which may stabilize carbon oxygenated groups and generate micropores. This assumption was further supported experimentally. Firstly, according to SEM-EDX analyses (**Table S3**), **IC-**

Fe-240 has more residual iron and chlorine than **HC-Fe-240**. Secondly, the simulated O1s XPS spectrum of **IC-Fe-240** (**Figure 4**, **Table S6**) suggests the presence of Fe-O species (contribution at 531 eV),[55] together with oxygen atoms in a strongly electronegative environment (contribution at 534.5 eV). The latter might refer to oxygen atoms in the second coordination sphere of $[FeCl_4]^-$ anions. These contributions are less pronounced for **HC-Fe-240** and **HC-240** (**Figure 4b-c**, **Table S6**). Additionally, the O/C mass ratio of **IC-Fe-240** extracted from XPS is significantly lower than the one obtained from elemental analysis (0.27 *vs.* 0.40 wt.% respectively, **Table S6**). This difference is less pronounced for **HC-Fe-240** and **HC-240**. This feature suggests that the carbonization at the biomass-solvent interface is more advanced than the carbonization in the bulk, especially for the ITC process in **BFe**. It also confirms the presence of oxygenated functional groups in the aromatic carbonaceous framework of **IC-Fe-240**, mainly due to the recalcitrant ligneous fractions.

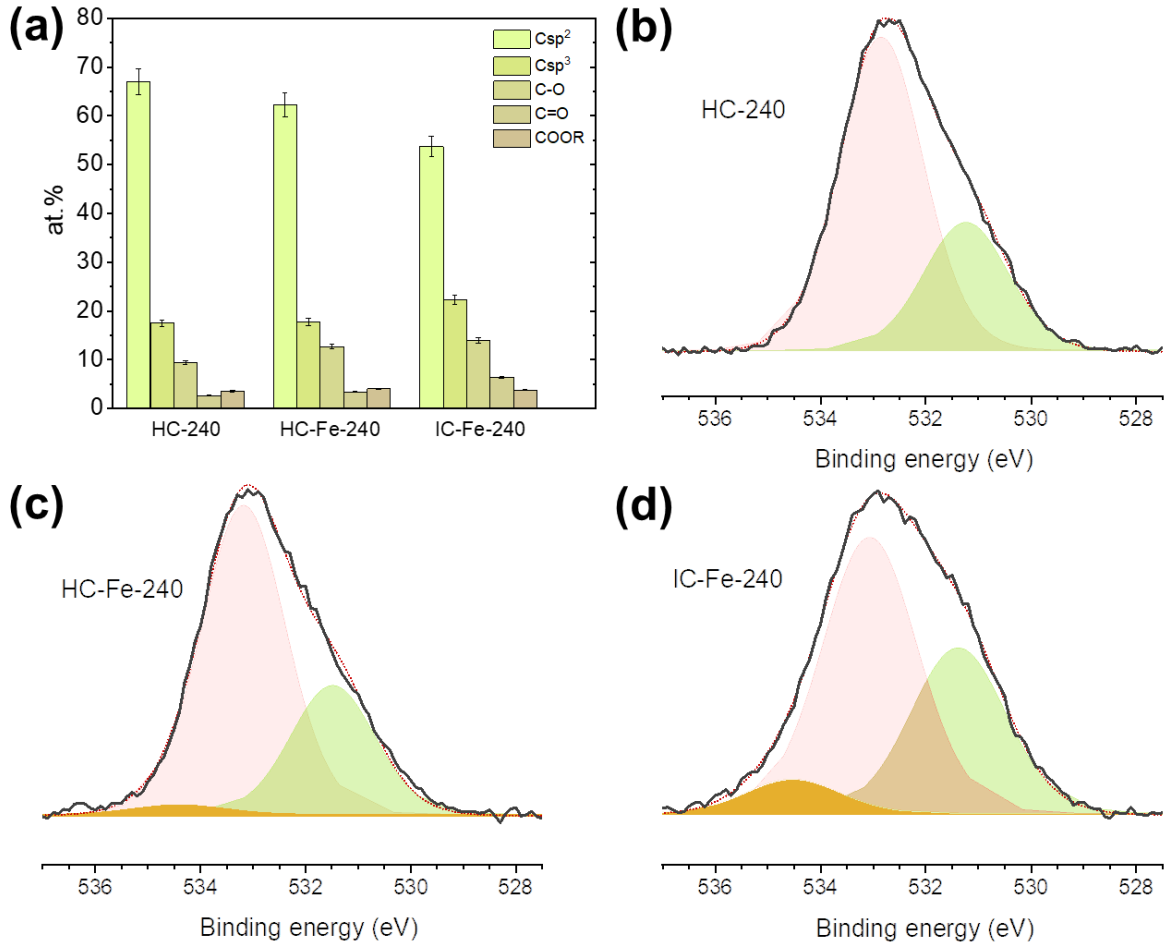

Figure 4. (a) XPS data obtained from the deconvoluted C1s spectra of **HC-240**, **HC-Fe-240** and **IC-Fe-240**. O1s XPS band-like spectra (black solid lines) and deconvoluted curves (colored filled curves) of (b) **HC-240**, (b) **HC-Fe-240** and (c) **IC-Fe-240**.

3.2. On the influence of hydration

At that stage, it is important to notice that ITC occurs under autogenous pressure induced by water produced during dehydration/condensation reactions and by low-boiling point organic by-products. The residual water present in IL and biomass might be also considered. In our case, **BFe** was thoroughly dried prior to ITC (water content c.a. 0 wt.% according to TGA, **Figure S6**) and the water content in CS was systematically controlled prior to thermochemical treatment (c.a. 7.5 wt.% according to TGA). As both IL and lignocellulosic biomass are usually hard to keep dry, we proposed to study the influence of water over the carbonization process and to explore the possibility to extend ITC to wet starting products and agrowastes. In our study, the bound water in CS represented an amount of c.a. 0.6 wt.% in relation to **BFe**. To study the influence of hydration, we conducted three experiments at 240°C for 20 hours at increasing water content in relation to **BFe** (2, 10 and 25 wt.%, corresponding to the ionochars named **IC-Fe-240-2w**, **IC-Fe-240-10w** and **IC-Fe-240-25w** respectively) and we compared with ITC (0 wt.%, **IC-Fe-240**) and HTC (100 wt.%, **HC-240**). The as-prepared ionochars were thoroughly characterized by elemental analyses (**Table S7**) and nitrogen sorption at 77 K (**Table S8**). The results are compiled in **Figure 5**. As shown in **Figure 5a**, **IC-Fe-240** and **IC-Fe-240-2w** depict similar mass and carbon yields of c.a. 43 and 73-75 wt.% respectively. While increasing the water content from 2 to 25 wt.%, mass and carbon yields significantly decreased to reach 38 and 62 wt.% respectively for **IC-Fe-240-25w**. This feature can be attributed to the decrease in iron-based Lewis catalysts while diluting **BFe**. Meanwhile, the textural properties of the ionochars were significantly affected by the water content. As shown in **Figure 5b**, all the samples, except for the one treated in 100 wt.% water (*i.e.*, **HC-240**), display a type I/II isotherm with a H3 hysteresis loop, related to micro-macroporous materials. Interestingly, both SSA_{BET} (**Table S8**) and pore volume (**Figure 5c**) reached a maximum for **IC-Fe-240-10w** of c.a. 616 $m^2.g^{-1}$ and 0.57 $cm^3.g^{-1}$ respectively. Particularly, a significant difference was observed for the contribution due to external pores (**Figure 5c**), *i.e.*, meso- and macropores in which the nitrogen adsorption occurs in multimolecular layers. While the micropore volume kept stable from **IC-Fe-240** to **IC-Fe-240-10w** with a value of c.a. 0.2 $cm^3.g^{-1}$, the external pore volume increased from 0.26 to 0.36 $cm^3.g^{-1}$ while increasing the water content from 0 to 10 wt.%. Reversely, while increasing the water content from 10 to 25 wt.%, the external pore volume drastically decreased to 0.2 $cm^3.g^{-1}$. As mentioned in **section 3.1**, **BFe** is amphiphilic and might form

complex liquid structures governed by the assembly of hydrophobic and hydrophilic domains. The addition of water may cause a change in the hydration state of **BFe** and modify the hydrophilic/hydrophobic balance that might affect these complex liquid structures. In our case, a small amount of water seems to be beneficial for the formation of ionic liquid nanodomains and, *in fine*, the generation of meso- and macropores in the ionochars. This result suggests that the use of wet starting products and agrowastes in the ITC process might be advantageous for the production of highly porous chars.

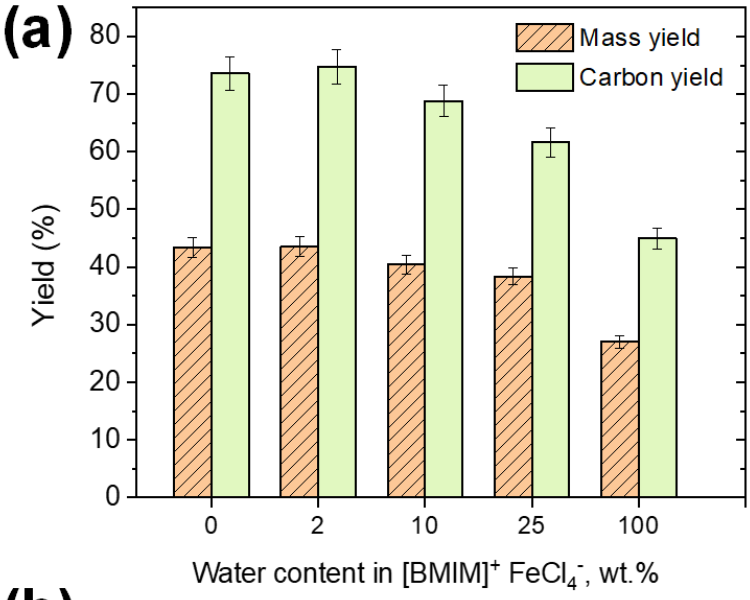
(a)
Mass yield
Carbon yield
Yield (%)
0
10
20
30
40
50
60
70
80
0
2
10
25
100
Water content in [BMIM]+ FeCl4-, wt.%

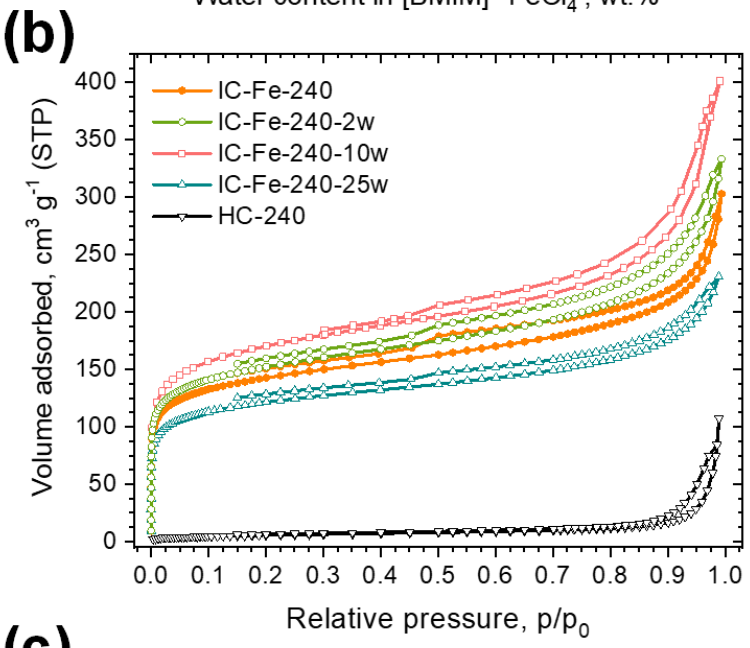
(b)
IC-Fe-240
IC-Fe-240-2w
IC-Fe-240-10w
IC-Fe-240-25w
HC-240
Volume adsorbed, cm3 g-1 (STP)
0
50
100
150
200
250
300
350
400
0.0
0.1
0.2
0.3
0.4
0.5
0.6
0.7
0.8
0.9
1.0
Relative pressure, p/p0

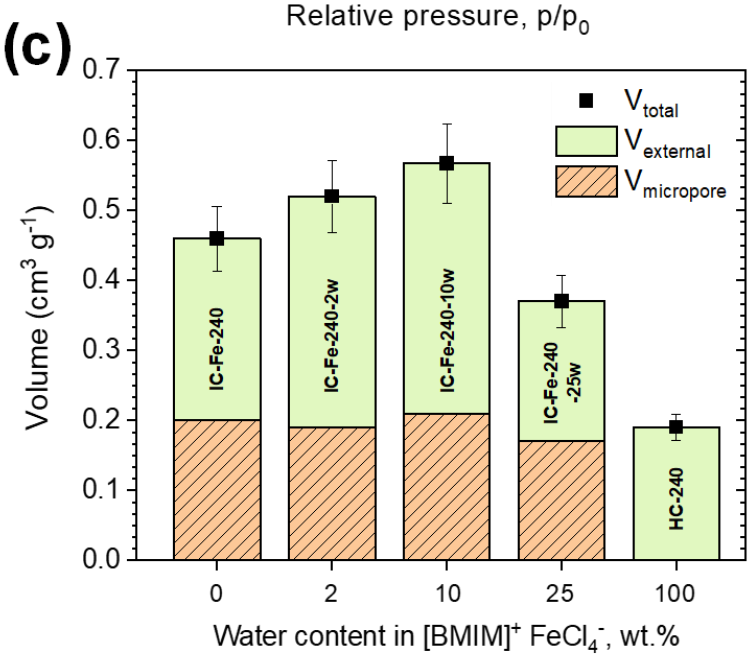
(c)
Vtotal
Vexternal
Vmicropore
Volume (cm3 g-1)
0.0
0.1
0.2
0.3
0.4
0.5
0.6
0.7
IC-Fe-240
IC-Fe-240-2w
IC-Fe-240-10w
IC-Fe-240 -25w
HC-240
0
2
10
25
100
Water content in [BMIM]+ FeCl4-, wt.%

Figure 5. (a) Mass and carbon yields, (b) Nitrogen sorption isotherms at 77 K and (c) pore volumes of **IC-Fe-240**, **IC-Fe-240-2w**, **IC-Fe-240-10w**, **IC-Fe-240-25w** and **HC-240**.

3.3. On the contribution of cellulosic and ligneous components

As mentioned in **section 3.1**, the ligneous fractions of CS seem to be mildly affected as compared to the cellulosic fractions. To get a better insight into the role of each component of the lignocellulosic material, commercial cellulose and kraft lignin were treated in **BFe** at 240°C for 20 hours, yielding **IC-Fe-240-C** and **IC-Fe-240-L** respectively. Those ionochars were compared with the ones obtained from raw CS (**IC-Fe-240**) and Klason lignin extracted from raw CS (**IC-Fe-240-KL**). The as-prepared ionochars were thoroughly characterized by elemental analyses (**Table S9**) and nitrogen sorption at 77 K (**Table S10**). The results are compiled in **Figure 6**. As shown in **Figure 6a**, the mass and carbon yields are significantly higher for ligneous materials than for cellulosic ones. This behavior can be explained by the fact that lignin contains more aromatic carbon and is more stable than hemicellulose and cellulose in these conditions. Regarding mass and carbon yields, CS and cellulose behaved similarly. This trend was confirmed by nitrogen sorption data. As shown in **Figure 6b**, **IC-Fe-240-C** and **IC-Fe-240** display similar type I/II isotherms with H3 hysteresis loops. **IC-Fe-240-C** shows, however, a larger SSA_{BET} of c.a. 736 $m^2.g^{-1}$ (550 $m^2.g^{-1}$ for **IC-Fe-240**) mainly due to micropores' contribution (**Table S10** and **Figure 6c**). Reversely, **IC-Fe-240-L** depicts a type II isotherm and is mainly macroporous with a low SSA_{BET} of c.a. 40 $m^2.g^{-1}$. Evidently, cellulose and hemicellulose, which undergo more severe structural rearrangement than lignin during the ITC process, contribute more quantitatively to the generation of micropores in the final ionochars. **IC-Fe-240-KL** depicts intermediate textural properties with a SSA_{BET} of c.a. 250 $m^2.g^{-1}$. The presence of residual carbohydrates or a higher H unit content in the Klason lignin extracted from CS as compared with the commercial Kraft lignin (**Figure S7**) might explain such difference. To elucidate this behavior, the ionothermal carbonization of different types of lignin and raw agrowastes is currently under investigation.

Another significant difference lies in the fact that **IC-Fe-240-L** contains twice more residual iron than the three other ionochars (*i.e.*, 6 wt.% *versus* c.a. 3 wt.% for the others, **Table S9**). As mentioned in **section 3.1**, $[FeCl_4]^-$ moieties are willing to coordinate to the oxygen atoms of carbohydrates and lignin. As reported by Li *et al.*,[48] the low absolute binding energy between the cation and the anion in **BFe** improves the efficient dissociation of $[Bmim]^+$ and $[FeCl_4]^-$ and favors the coordination interactions between Fe atom of $[FeCl_4]^-$

and O atom of ester and phenol groups from lignin. One may assume that the recalcitrant G and S units in lignin[48] are willing to form stable coordination complexes with $[FeCl_4]^-$ and to trap more iron atoms in the final carbonaceous framework.

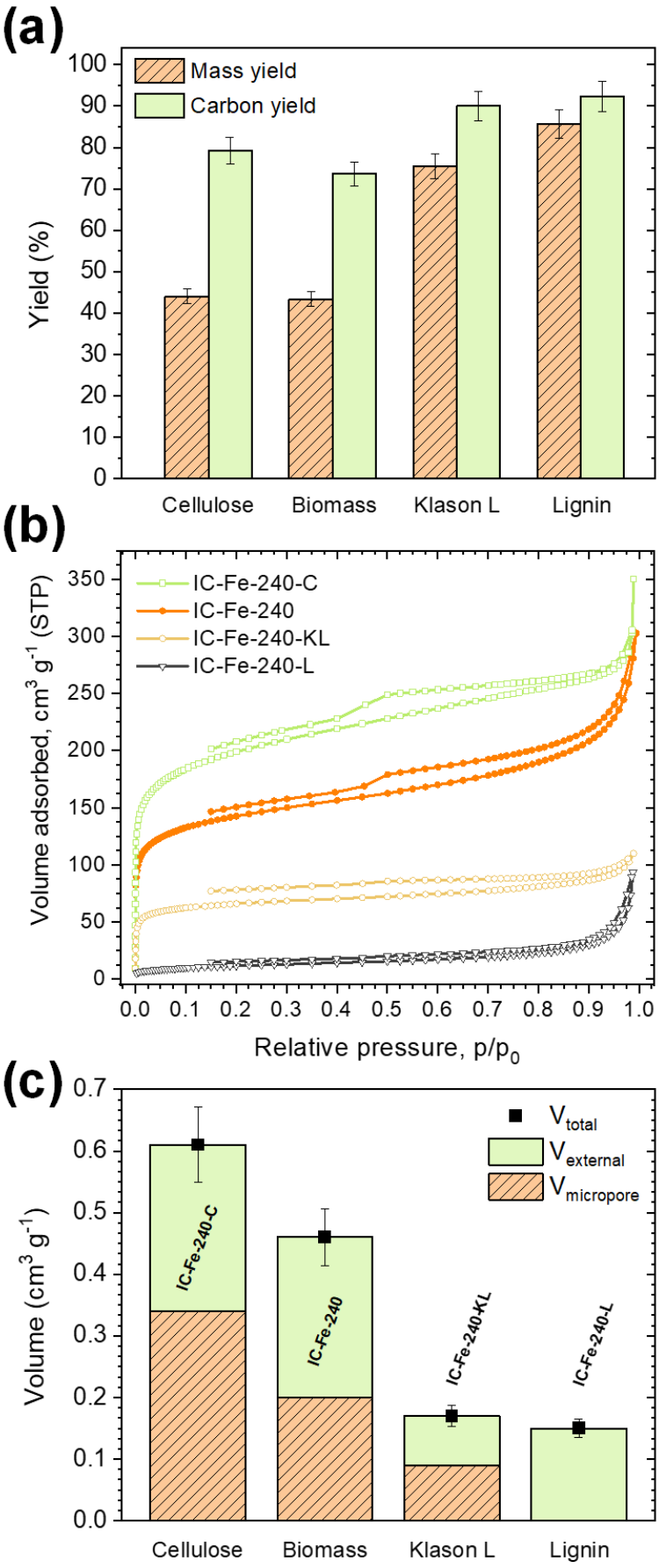
(a)
Mass yield
Carbon yield
Yield (%)
0
10
20
30
40
50
60
70
80
90
100
Cellulose
Biomass
Klason L
Lignin
(b)
IC-Fe-240-C
IC-Fe-240
IC-Fe-240-KL
IC-Fe-240-L
Volume adsorbed, cm3 g-1 (STP)
0
50
100
150
200
250
300
350
0.0
0.1
0.2
0.3
0.4
0.5
0.6
0.7
0.8
0.9
1.0
Relative pressure, p/p0
(c)
Vtotal
Vexternal
Vmicropore
Volume (cm3 g-1)
0.0
0.1
0.2
0.3
0.4
0.5
0.6
0.7
IC-Fe-240-C
IC-Fe-240
IC-Fe-240-KL
IC-Fe-240-L
Cellulose
Biomass
Klason L
Lignin

Figure 6. (a) Mass and carbon yields, (b) Nitrogen sorption isotherms at 77 K and (c) pore volumes of **IC-Fe-240**, **IC-Fe-240-C**, **IC-Fe-240-L** and **IC-Fe-240-KL**.

3.4. Recyclability and reusability of [Bmim][$FeCl_4$]

To support the sustainability of the ITC process, the recyclability of **BFe** was investigated. The iron-containing ionic liquid was thoroughlty characterized by FTIR spectroscopy and ICP atomic emission spectrometry (ICP-AES) before (**BFe**) and after ITC of raw CS at 180 and 240°C for 20 hours (**BFe-r180** and **BFe-r240** respectively, **Figure 7a**). While the chemical signature of [Bmim][$FeCl_4$] was preserved, the amount of iron decreased from 16.6 wt.% in fresh **BFe** to 16.3 wt.% in **BFe-r180** and 16.0 wt.% in **BFe-r240**. This result confirms the loss of iron during ITC, partly due to the presence of remaining $[FeCl_4]^-$ complexes in ionochars. One may also consider the fact that both **BFe-r180** and **BFe-r240** were collected only after the first filtration step, which allowed recovering c.a. 95 wt.% of the IL. $[FeCl_4]^-$ moieties and imidazolium cations were also present in the subsequent filtrates, making the recycling largely improvable. **BFe-r240** was also characterized by GC-MS and no degradation products were detected, while imidazole by-products (e.g., imidazole, methylimidazole, 1-butylimidazole and N-Propionylimidazole) were identified for [Bmim]Cl recovered after ITC of CS at 240°C (**Figure S3**). These by-products were probably generated by the cleavage of the butyl and methyl side chains by hydroxyl radicals.[56] **BFe-r240** was reused for the ITC of CS at 240°C for 20 hours, yielding **IC-Fe-240-r1**. This ionochar was compared with **IC-Fe-240** (**Tables S11** and **S12**). As shown in **Figure 7b**, **IC-Fe-240** and **IC-Fe-240-r1** display similar type I/II isotherms with H3 hysteresis loops. Meanwhile, the mass and carbon yields were not affected (**Figure 7c**). However, the SSA_{BET} slightly decreased from 550 $m^2.g^{-1}$ for **IC-Fe-240** to 455 $m^2.g^{-1}$ for **IC-Fe-240-r1** (**Table S12**). This difference results from a reduction in the micropore contribution (**Figure 7d**), which is mainly related to the amount of $[FeCl_4]^-$ moieties in the reaction medium as mentioned above.

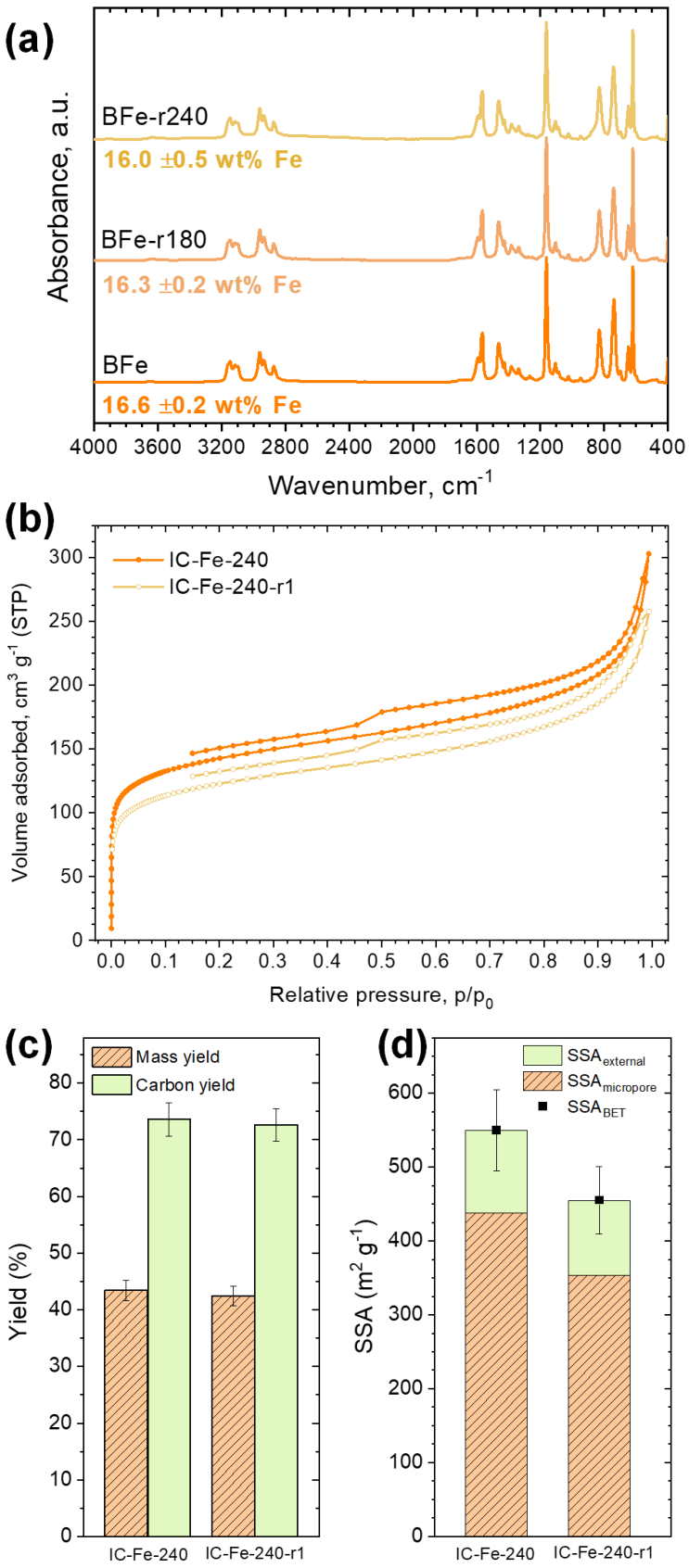
(a)
Absorbance, a.u.
BFe-r240
16.0 ±0.5 wt% Fe
BFe-r180
16.3 ±0.2 wt% Fe
BFe
16.6 ±0.2 wt% Fe
4000 3600 3200 2800 2400 2000 1600 1200 800 400
Wavenumber, cm-1
(b)
IC-Fe-240
IC-Fe-240-r1
Volume adsorbed, cm3 g-1 (STP)
0 50 100 150 200 250 300
0.0 0.1 0.2 0.3 0.4 0.5 0.6 0.7 0.8 0.9 1.0
Relative pressure, p/p0
(c)
Mass yield
Carbon yield
Yield (%)
0 10 20 30 40 50 60 70 80
IC-Fe-240
IC-Fe-240-r1
(d)
SSAexternal
SSAmicropore
SSABET
SSA (m2 g-1)
0 100 200 300 400 500 600
IC-Fe-240
IC-Fe-240-r1

Figure 7. (a) FTIR spectra of **BFe**, **BFe-r180** and **BFe-r240**. (b) Nitrogen sorption isotherms at 77 K of **IC-Fe-240** and **IC-Fe-240-r1**. (c) Yields and (d) specific surface areas of **IC-Fe-240** and **IC-Fe-240-r1**.

3.5. Pyrolysis and CO_2 activation: from ionochars to activated carbons

High temperature post-treatments (*i.e.*, pyrolysis and CO_2 activation) were carried out on ionochars to further investigate their potential and extend their applicability. After pyrolysis at 900°C under argon (**P9** series), porous carbon materials with increased carbon content (c.a. 90 wt.%) can be obtained (**Tables S13 and S14**). Interestingly, the remnant of iron in ionochars was converted to iron-carbon core-shell nanoparticles as shown by high-resolution TEM imaging (**Figure 8a**) and elemental EDX mapping (**Figure 8b** and **Figure S8**). According to X-ray diffraction performed on **IC-Fe-240-P9** (**Figure 8c**), the core of these core-shell nanoparticles is composed of iron (α-Fe), iron carbide (Fe_3C), and maghemite (γ-Fe_2O_3). TEM imaging also revealed that highly ordered graphitic layers surround the iron-based core (**Figure S9**). The carbothermal reduction of iron salts to α-Fe and Fe_3C at high temperature and the formation of similar core-shell structures were already described for biomass derived hydrochars[57] and ionochars[42]. As a direct consequence, these ionochar-derived carbons are strongly attracted to magnets (insert in **Figure 8a**) and might be easily separable from solution by external magnetic fields. Besides, the textural properties of the ionochars were mainly preserved after pyrolysis, with type I/II isotherms with H3 hysteresis loops and a slight increase in micropore contributions (**Table S13** and **Figure 9a**). Based on these advantageous properties, we are currently investigating their use in magnetic separation for wastewater treatment and depollution.

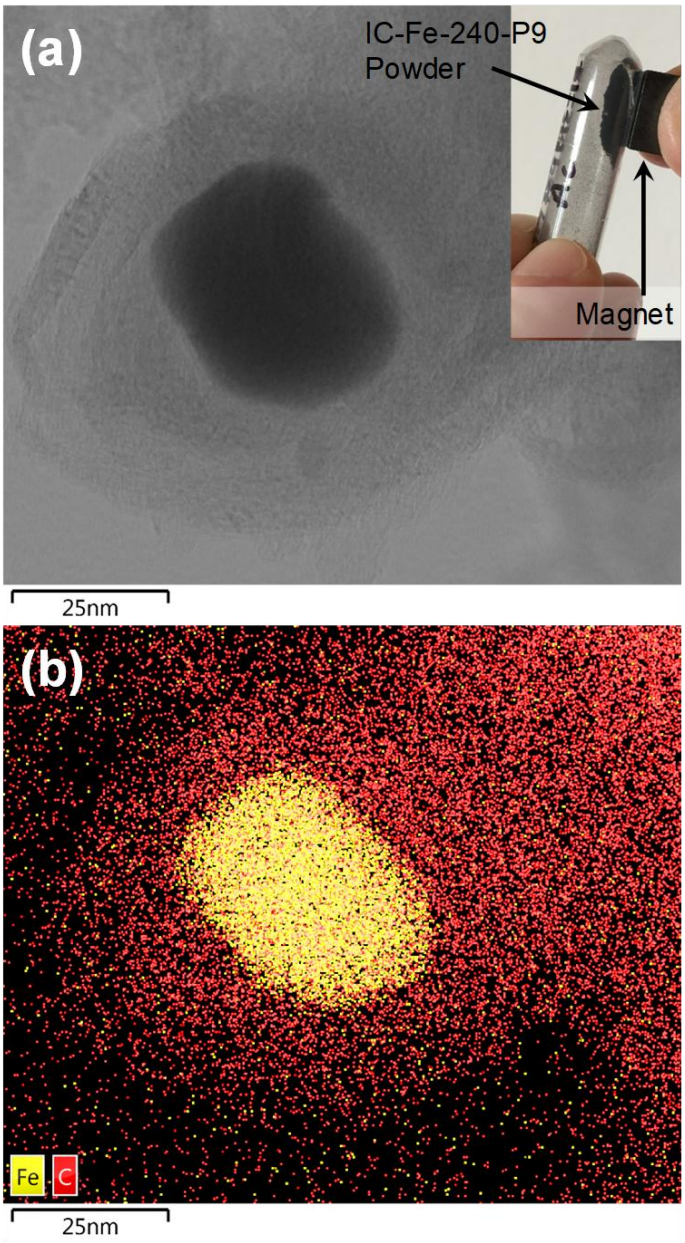
(a)
IC-Fe-240-P9
Powder
Magnet
25nm
(b)
Fe
C
25nm
(c)
Fe3C / Fe
γ-Fe2O3
Fe3C
IC-Fe-240-P9
IC-Fe-240
Counts (a.u.)
10
15
20
25
30
35
40
45
50
55
60
2θ (°)

Figure 8. (a) HR-TEM micrograph and (b) STEM-EDX mapping of a core-shell structure observed in **IC-Fe-240-P9**. (c) XRD patterns of **IC-Fe-240** and **IC-Fe-240-P9**. The upper right insert is a picture of **IC-Fe-240-P9** attracted to a magnet.

To evaluate the potential of ITC as a pretreatment for the preparation of highly porous carbons (*i.e.*, activated carbons), we also studied the physical activation of a few samples under a CO_2-rich atmosphere at 950°C. HTC has been established as an efficient pretreatment in the transformation of carbohydrates and raw lignocellulosic biomass to activated carbons.[9, 10] Recently, Xie *et al.*[46] also proposed to use ITC as an intermediate step prior to activation of raw biomass. All these studies used KOH activation at high temperature (between 600 and 900°C). The latter is a chemical activation commonly employed to prepare activated carbons with high SSA and narrow micropores.[58] In this study, we proposed to investigate another approach, *i.e.* the physical activation in a CO_2-rich atmosphere. CO_2 activation has been less employed than KOH activation as it usually yields activated carbons with lower SSA. Nonetheless, CO_2 activation usually offers higher yields and carbon content compared to chemical activation.[58] Moreover, CO_2 activation is more advantageous in terms of time, cost and simplicity.[58]

Two samples were submitted to CO_2 activation at 950°C: **HC-240**, the hydrochar serving as a reference; and **IC-Fe-240-10w**, the ionochar with the highest SSA_{BET}. Two different procedures were employed: **A1**, when the samples were submitted to CO_2 activation for 2 hours at the plateau only; and **A2**, when the sample was submitted to CO_2 activation from the beginning of the heating ramp, starting from 110°C. As shown in **Figure 9b**, the activated carbons still display type I/II isotherms. Both pore volumes and SSA_{BET} were significantly increased as compared with the carbons obtained by pyrolysis (**P9** series, **Table S15**). Considering textural properties, ITC seems to be favorable compared to HTC. After a similar activation procedure (**A1**), **IC-Fe-240-10w-A1** presents a SSA_{BET} of c.a. 1440 $m^2.g^{-1}$, mainly due to micropores' contribution ($SSA_{micropore}$ of c.a. 1200 $m^2.g^{-1}$), while **HC-240-A1** presents a SSA_{BET} of c.a. 800 $m^2.g^{-1}$ (**Table S15**). Meanwhile, the activation procedure **A2** allows reaching higher SSA. Thus, **IC-Fe-240-10w-A2** presents a SSA_{BET} of c.a. 2060 $m^2.g^{-1}$, with a micropores' contribution of c.a. 1800 $m^2.g^{-1}$. Interestingly, mass yields of 35-44 wt.% were obtained (**Table S16**).

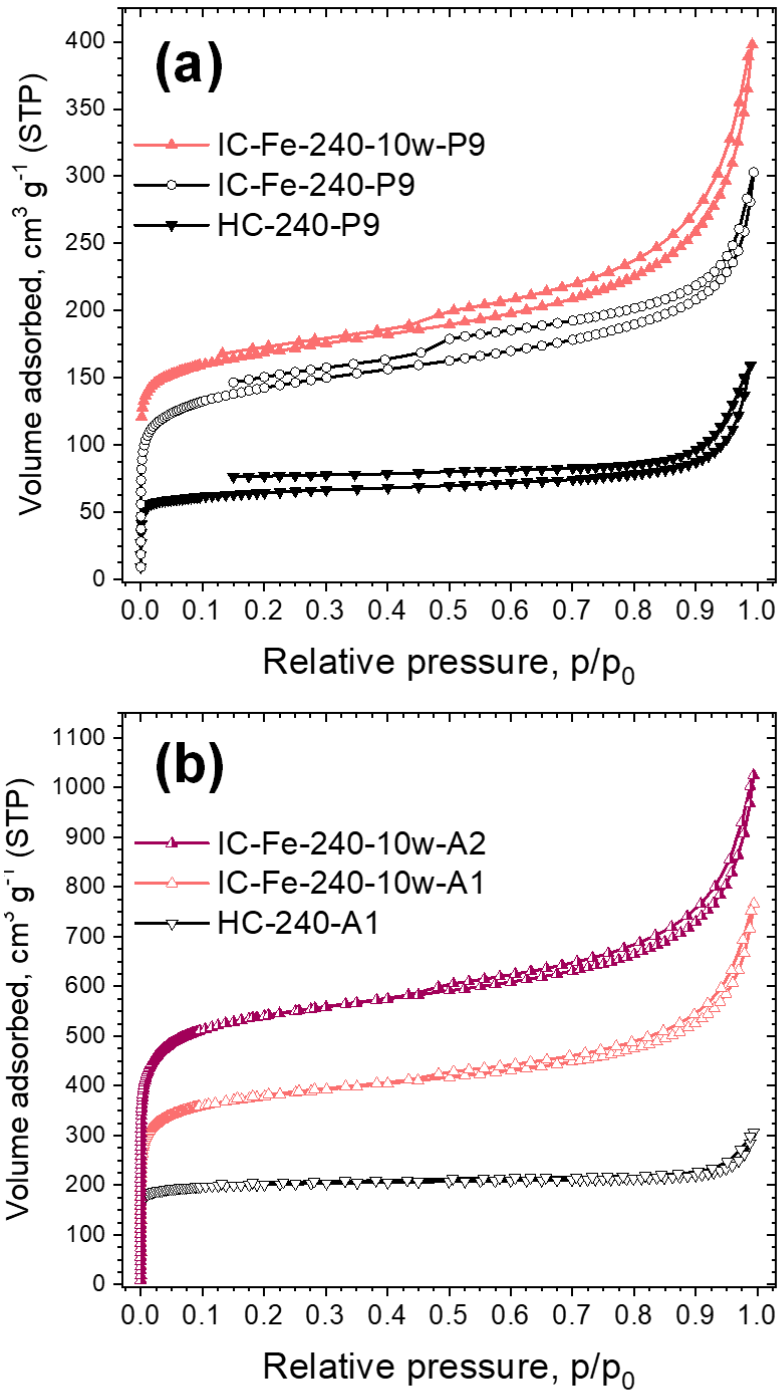

Figure 9. Nitrogen sorption isotherms at 77 K of some ionochars after (a) pyrolysis at 900°C under argon and (b) CO_2 activation at 950°C.

3.6. Preliminary results for post combustion CO_2 capture

The hydrochars, ionochars and carbons prepared in this study were tested for post combustion CO_2 capture. The most representative isotherms recorded at 273 K are shown in **Figure 10a**. For a purpose of comparison, the CO_2 uptakes of each sample are represented in **Figure 10b** as a function of their corrected mass yield. We believe that these two parameters, *i.e.*, mass yield and CO_2 uptake, are crucial to evaluate both the efficiency and the sustainability of the different materials prepared in this study. Interestingly, two regions can be clearly identified. The ionochars and ionochar-derived carbons gather in the upper right region, which corresponds to higher mass yields and/or higher CO_2 uptakes. Reversely, all the other materials gather in the bottom left region, which corresponds to lower mass yields and/or lower CO_2 uptakes. In another representation, we proposed to express the CO_2 uptakes of each sample per gram of CS treated, *i.e.* the CO_2 uptakes were weighted as a function of the total mass yields of each activation procedure. The same trend was observed (**Figure S10**). The ionochars and ionochar-derived carbons display weighted CO_2 uptakes superior to 0.8 mmol of CO_2 adsorbed per gram of CS treated, while the other materials were below 0.6 $mmol.g^{-1}$. These results further demonstrate that ITC in [Bmim][$FeCl_4$] is an advantageous pretreatment for the transformation of raw lignocellulosic agrowastes into advanced activated carbons for CO_2 capture.

The CO_2 uptake of the most efficient material, *i.e.*, **IC-Fe-240-10w-A2**, was also tested at 293 and 298 K (**Figure 10c**). At 298 K and 1 bar, **IC-Fe-240-10w-A2** was able to adsorb 4.4 mmol of CO_2 per gram. This value is amongst the highest values reported to date in literature for nitrogen-free biomass-derived carbons (**Table 1**).[8-10, 58] To the best of our knowledge, it's also the highest CO_2 uptake reported to date for CO_2 activated biomass-derived carbons.[58, 59] These results are highly promising and might encourage further studies in the field of ionochars-derived activated carbons. With this aim, we are currently investigating different chemical activation procedures (KOH and $ZnCl_2$) to produce ionochars-derived carbons with enhanced micropores' contribution. Thorough characterizations of the CO_2 adsorbents reported here are also under investigation such as cyclic stability, adsorption kinetics, and CO_2/N_2 selectivity. Considering the advantageous textural properties of these materials, precombustion CO_2 capture at higher pressure should be also considered.

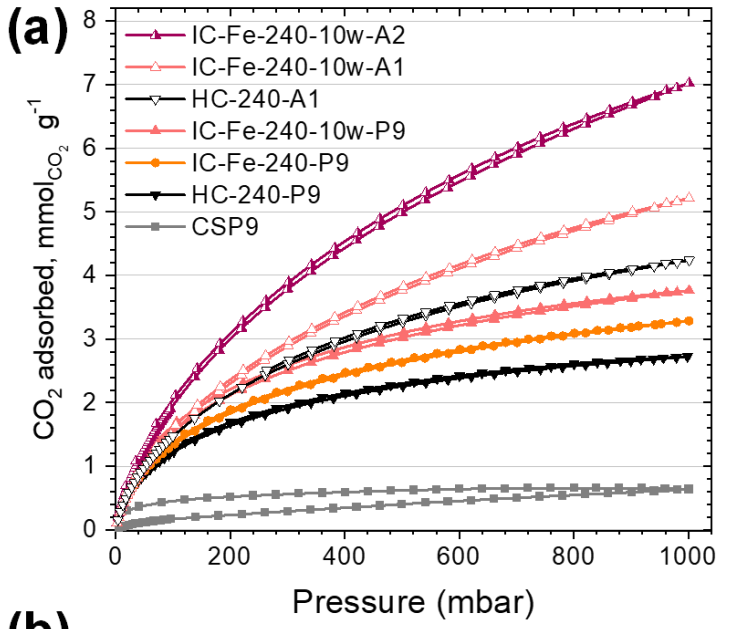
(a)
IC-Fe-240-10w-A2
IC-Fe-240-10w-A1
HC-240-A1
IC-Fe-240-10w-P9
IC-Fe-240-P9
HC-240-P9
CSP9
CO2 adsorbed, mmolCO2 g-1
Pressure (mbar)

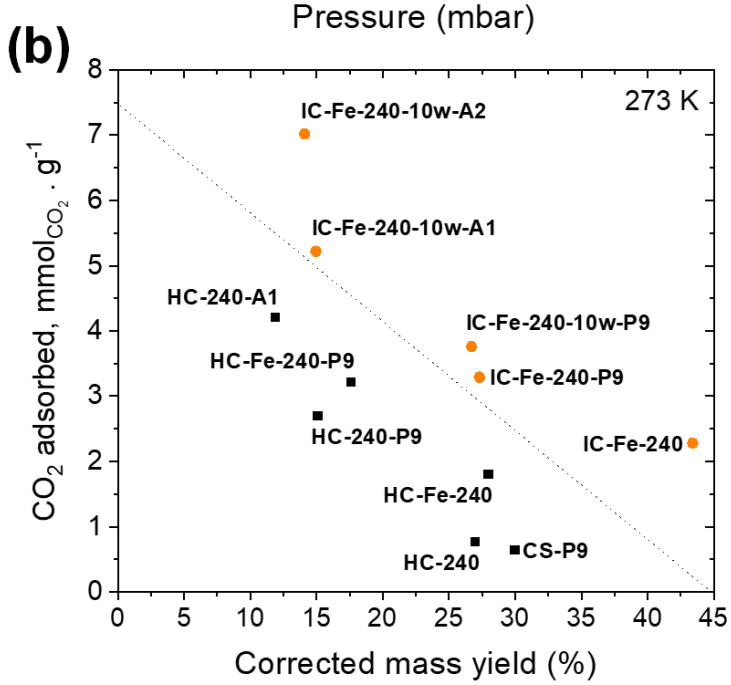
(b)
273 K
IC-Fe-240-10w-A2
IC-Fe-240-10w-A1
HC-240-A1
IC-Fe-240-10w-P9
HC-Fe-240-P9
IC-Fe-240-P9
HC-240-P9
IC-Fe-240
HC-Fe-240
HC-240
CS-P9
CO2 adsorbed, mmolCO2 . g-1
Corrected mass yield (%)

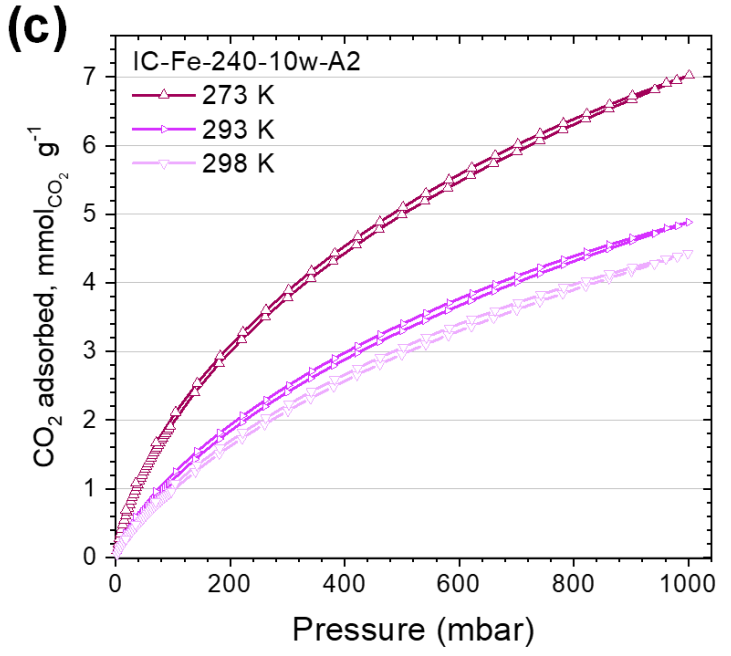
(c)
IC-Fe-240-10w-A2
273 K
293 K
298 K
CO2 adsorbed, mmolCO2 g-1
Pressure (mbar)

Figure 10. (a) CO_2 sorption isotherms at 273 K of some ionochars after pyrolysis or CO_2 activation. **(b)** CO_2 uptake at 273 K and 1 bar expressed in $mmol.g^{-1}$ as a function of the corrected mass yield of the hydrochars, ionochars and carbons prepared in this study. **(c)** CO_2 sorption isotherms at 273, 293 and 298 K of **IC-Fe-240-10w-A2**.

Table 1. A selection of nitrogen-free biomass-derived carbons that have amongst the highest CO_2 uptake values reported to date in literature for post combustion CO_2 capture at 298 K. CO_2 activated carbons are highlighted in grey. ‡ Values related to **IC-Fe-240-10w-A2**.

Biomass	Pretreatment	Activation	SSA_{BET} ($m^2 . g^{-1}$)	CO_2 uptake at 298 K ($mmol.g^{-1}$)		Reference
				0.15 bar	1 bar	
Cocoa bean shells	ITC	CO_2 950°C	2060	1.3	4.4	Our study‡
Sawdust	n/a	KOH 700°C	1575	1.3	4.6	8
Camellia japonica	HTC	KOH 700°C	1353	1.5	5.0	9
Sawdust	HTC	KOH 600°C	1260	n/a	4.8	10
Date stones	n/a	KOH 800°C	2367	1.1	4.4	60
Grass cuttings	HTC	CO_2 800°C	841	1.1	2.8	61
Coconut shells	n/a	CO_2 800°C	1327	n/a	3.9	62
Olive stones	n/a	CO_2 800°C	1215	n/a	3.1	63

4. Conclusion

In this study, we investigated the ITC of a raw lignocellulosic agrowaste used as a model, *i.e.* cocoa bean shells from Cameroon, in [Bmim][$FeCl_4$]. The beneficial inputs of the ITC approach in [Bmim][$FeCl_4$] towards mass yield, carbon yield and specific surface area were clearly evidenced. The coordination of $[FeCl_4]^-$ to the oxygen atoms of lignocellulosic materials and ionochars seems to stabilize carbon oxygenated groups – accounting for enhanced mass and carbon yields – and to favor the generation of micropores. The influence of hydration over yields and textural properties was also investigated. We showed that the use of wet starting products and agrowastes in the ITC process might be advantageous for the production of highly porous chars. Importantly, the contributions of lignin and cellulose were

highlighted and the recyclability of [Bmim][$FeCl_4$] was clearly evidenced, proving the sustainability of the ITC approach and making this process easily applicable to other raw agrowastes. The subsequent activation of the as-obtained ionochars with carbon dioxide allowed producing activated carbons with specific surface area superior to 2000 $m^2.g^{-1}$ and remarkable CO_2 uptake as high as 4.4 $mmol.g^{-1}$ at 25°C and 1 bar. This value is the highest CO_2 uptake reported to date in literature for CO_2 activated biomass-derived carbons. To conclude, this work highlights the numerous advantages offered by the ionothermal carbonization for the valorization of raw lignocellulosic agrowastes into advanced porous carbons.

Conflicts of Interest

There are no conflicts to declare.

Acknowledgements

This project was supported by Chimie Balard Cirimat Carnot institute through the ANR program N°16 CARN 0008-01. This work was partially supported by INSA Rouen, Rouen University, CNRS, Labex SynOrg (ANR-11-LABX-0029). Several characterizations were performed with the support of the "Balard Plateforme d'Analyses et de Caractérisation (PAC Balard)". The authors would like to thank Didier Cot for SEM, Bertrand Rebière for SEM-EDX, Franck Godiard for TEM, Erwan Oliviero for STEM-EDX, Christine Biolley for ICP-AES, Pascale Guiffrey for GC-MS, Thomas Cacciaguerra for XRD and Emmanuel Fernandez for solid-state NMR.

Notes and references

1. M. J. Climent, A. Corma and S. Iborra, *Green Chem*, 2014, **16**, 516-547.
2. N. Brun, P. Hesemann and D. Esposito, *Chem Sci*, 2017, **8**, 4724-4738.
3. M. M. Titirici, R. J. White, N. Brun, V. L. Budarin, D. S. Su, F. del Monte, J. H. Clark and M. J. MacLachlan, *Chem Soc Rev*, 2015, **44**, 250-290.
4. R. J. White, N. Brun, V. L. Budarin, J. H. Clark and M. M. Titirici, *Chemsuschem*, 2014, **7**, 670-689.
5. H. Lu and X. S. Zhao, *Sustainable Energy & Fuels*, 2017, **1**, 1265-1281.
6. C. Falco, J. M. Sieben, N. Brun, M. Sevilla, T. van der Mauelen, E. Morallon, D. Cazorla-Amoros and M. M. Titirici, *Chemsuschem*, 2013, **6**, 374-382.
7. M. Soorholtz, R. J. White, T. Zimmermann, M. M. Titirici, M. Antonietti, R. Palkovits and F. Schuth, *Chem Commun*, 2013, **49**, 240-242.
8. N. Balahmar, A. S. Al-Jumialy and R. Mokaya, *J Mater Chem A*, 2017, **5**, 12330-12339.
9. H. M. Coromina, D. A. Walsh and R. Mokaya, *J Mater Chem A*, 2016, **4**, 280-289.
10. M. Sevilla and A. B. Fuertes, *Energ Environ Sci*, 2011, **4**, 1765-1771.

11. H. Wikberg, T. Ohra-aho, F. Pileidis and M. M. Titirici, *Acs Sustain Chem Eng*, 2015, **3**, 2737-2745.
12. C. Falco, F. P. Caballero, F. Babonneau, C. Gervais, G. Laurent, M. M. Titirici and N. Baccile, *Langmuir*, 2011, **27**, 14460-14471.
13. C. Falco, N. Baccile and M. M. Titirici, *Green Chem*, 2011, **13**, 3273-3281.
14. M. M. Titirici and M. Antonietti, *Chem Soc Rev*, 2010, **39**, 103-116.
15. M. M. Titirici, M. Antonietti and N. Baccile, *Green Chem*, 2008, **10**, 1204-1212.
16. M. M. Titirici, A. Thomas and M. Antonietti, *New J Chem*, 2007, **31**, 787-789.
17. H. L. Wang, Z. Li, J. K. Tak, C. M. B. Holt, X. H. Tan, Z. W. Xu, B. S. Amirkhiz, D. Hayfield, A. Anyia, T. Stephenson and D. Mitlin, *Carbon*, 2013, **57**, 317-328.
18. M. M. Titirici, A. Thomas and M. Antonietti, *Adv Funct Mater*, 2007, **17**, 1010-1018.
19. L. H. Yu, N. Brun, K. Sakaushi, J. Eckert and M. M. Titirici, *Carbon*, 2013, **61**, 245-253.
20. N. Brun, L. Edembe, S. Gounel, N. Mano and M. M. Titirici, *Chemsuschem*, 2013, **6**, 701-710.
21. N. Brun, K. Sakaushi, L. H. Yu, L. Giebeler, J. Eckert and M. M. Titirici, *Phys Chem Chem Phys*, 2013, **15**, 6080-6087.
22. S. Kubo, R. J. White, K. Tauer and M. M. Titirici, *Chem Mater*, 2013, **25**, 4781-4790.
23. R. J. White, K. Tauer, M. Antonietti and M. M. Titirici, *J Am Chem Soc*, 2010, **132**, 17360-17363.
24. N. Brun, C. A. Garcia-Gonzalez, I. Smirnova and M. M. Titirici, *Rsc Adv*, 2013, **3**, 17088-17096.
25. R. J. White, N. Yoshizawa, M. Antonietti and M. M. Titirici, *Green Chem*, 2011, **13**, 2428-2434.
26. T. P. Fellinger, R. J. White, M. M. Titirici and M. Antonietti, *Adv Funct Mater*, 2012, **22**, 3254-3260.
27. N. Brun, S. A. Wohlgemuth, P. Osiceanu and M. M. Titirici, *Green Chem*, 2013, **15**, 2514-2524.
28. R. P. Swatloski, S. K. Spear, J. D. Holbrey and R. D. Rogers, *J Am Chem Soc*, 2002, **124**, 4974-4975.
29. S. Barthel and T. Heinze, *Green Chem*, 2006, **8**, 301-306.
30. T. Heinze, K. Schwikal and S. Barthel, *Macromol Biosci*, 2005, **5**, 520-525.
31. H. Zhao, G. A. Baker, Z. Y. Song, O. Olubajo, T. Crittle and D. Peters, *Green Chem*, 2008, **10**, 696-705.
32. H. Zhang, J. Wu, J. Zhang and J. S. He, *Macromolecules*, 2005, **38**, 8272-8277.
33. R. C. Remsing, R. P. Swatloski, R. D. Rogers and G. Moyna, *Chem Commun*, 2006, 1271-1273.
34. H. Wang, G. Gurau and R. D. Rogers, *Chem Soc Rev*, 2012, **41**, 1519-1537.
35. B. L. Lu, A. R. Xu and J. J. Wang, *Green Chem*, 2014, **16**, 1326-1335.
36. A. M. D. Lopes and R. Bogel-Lukasik, *Chemsuschem*, 2015, **8**, 947-965.
37. S. R. Wang, Y. Zhao, H. Z. Lin, J. P. Chen, L. J. Zhu and Z. Y. Luo, *Green Chem*, 2017, **19**, 3869-3879.
38. H. Z. Lin, J. P. Chen, Y. Zhao and S. R. Wang, *Energ Fuel*, 2017, **31**, 3929-3934.
39. P. F. Zhang, J. Y. Yuan, T. P. Fellinger, M. Antonietti, H. R. Li and Y. Wang, *Angew Chem Int Edit*, 2013, **52**, 6028-6032.
40. S. Y. Wu, Y. S. Ding, X. M. Zhang, H. O. Tang, L. Chen and B. X. Li, *J Solid State Chem*, 2008, **181**, 2171-2177.
41. J. S. Lee, R. T. Mayes, H. M. Luo and S. Dai, *Carbon*, 2010, **48**, 3364-3368.
42. Z. L. Xie, R. J. White, J. Weber, A. Taubert and M. M. Titirici, *J Mater Chem*, 2011, **21**, 7434-7442.
43. Z. L. Xie, X. Huang, M. M. Titirici and A. Taubert, *Rsc Adv*, 2014, **4**, 37423-37430.
44. X. X. Lin, B. Tan, L. Peng, Z. F. Wu and Z. L. Xie, *J Mater Chem A*, 2016, **4**, 4497-4505.
45. P. F. Zhang, Y. T. Gong, Z. Z. Wei, J. Wang, Z. Y. Zhang, H. R. Li, S. Dai and Y. Wang, *Acs Appl Mater Inter*, 2014, **6**, 12515-12522.
46. Y. C. Liu, B. B. Huang, X. X. Lin and Z. L. Xie, *J Mater Chem A*, 2017, **5**, 13009-13018.
47. T. Zhang, Y. Q. Zhang, Y. L. Wang, F. Huo, Z. M. Li, Q. Zang, H. Y. He and X. H. Li, *Front Chem*, 2019, **7**.

48. Z. M. Li, Z. P. Cai, Q. Zeng, T. Zhang, L. J. France, C. H. Song, Y. Q. Zhang, H. Y. He, L. L. Jiang, J. X. Long and X. H. Li, *Green Chem*, 2018, **20**.
49. Z. S. Vasquez, L. P. D. Neto, G. V. M. Pereira, L. P. S. Vandenberghe, P. Z. de Oliveira, P. B. Tiburcio, H. L. G. Rogez, A. G. Neto and C. R. Soccol, *Waste Manage*, 2019, **90**, 72-83.
50. S. Bhagia, A. Nunez, C. E. Wyman and R. Kumar, *Bioresource Technol*, 2016, **216**, 1077-1082.
51. S. Hayashi and H. O. Hamaguchi, *Chem Lett*, 2004, **33**, 1590-1591.
52. M. El Achaby, N. Fayoud, M. C. Figueroa-Espinoza, H. Ben Youcef and A. Aboulkas, *Rsc Adv*, 2018, **8**, 5212-5224.
53. D. C. G. Okiyama, S. L. B. Navarro and C. E. C. Rodrigues, *Trends Food Sci Tech*, 2017, **63**, 103-112.
54. J. G. Li, Y. F. Hu, S. F. Sun, S. Ling and J. Z. Zhang, *J Phys Chem B*, 2012, **116**, 6461-6464.
55. L. W. Yang, L. L. Han, J. Ren, H. L. Wei and L. Y. Jia, *Colloid Surface A*, 2015, **484**, 197-205.
56. A. Fabianska, T. Ossowski, P. Stepnowski, S. Stolte, J. Thoming and E. M. Siedlecka, *Chem Eng J*, 2012, **198**, 338-345.
57. S. T. Neeli and H. Ramsurn, *Carbon*, 2018, **134**, 480-490.
58. G. Singh, K. S. Lakhi, S. Sil, S. V. Bhosale, I. Kim, K. Albahily and A. Vinu, *Carbon*, 2019, **148**, 164-186.
59. S. Jung, Y. K. Park and E. E. Kwon, *J Co2 Util*, 2019, **32**, 128-139.
60. J. X. Li, B. Michalkiewicz, J. K. Min, C. D. Ma, X. C. Chen, J. Gong, E. Mijowska and T. Tang, *Chem Eng J*, 2019, **360**, 250-259.
61. W. M. Hao, E. Bjorkman, M. Lilliestrale and N. Hedin, *Appl Energ*, 2013, **112**, 526-532.
62. A. S. Ello, L. K. C. de Souza, A. Trokourey and M. Jaroniec, *Micropor Mesopor Mat*, 2013, **180**, 280-283.
63. A. S. Gonzalez, M. G. Plaza, F. Rubiera and C. Pevida, *Chem Eng J*, 2013, **230**, 456-465.